Analysis of properties of the 19 February 2018 volcanic eruption of Mount Sinabung in S5P/TROPOMI and Himawari satellite data

Adrianus de Laat[1], Margarita Vazquez-Navarro[2], Nicolas Theys[3], and Piet Stammes[1]

[1]KNMI, de Bilt, 3731 GK, the Netherlands
[2]DLR, Oberpfaffenhofen, D-82234 Wessling, Germany (currently at EUMETSAT)
[3]Royal Belgian Institute for Space Aeronomy (BIRA-IASB), Brussels, 1180, Belgium

Correspondence to: Jos de Laat (laatdej@knmi.nl)

Abstract. This study presents an analysis of TROPOMI cloud heights as a proxy for volcanic plume heights in the presence of absorbing aerosols and sulfur dioxide for the 19 February 2018 eruption plume of the Sinabung volcano on Sumatra, Indonesia.

Comparison with CALIPSO satellite data shows that all three TROPOMI cloud height data products based on oxygen absorption which are considered here (FRESCO, ROCINN, O22CLD) provide volcanic ash heights comparable to heights measured by CALIPSO for optically thick volcanic ash clouds. FRESCO and ROCINN heights are very similar with only differences for FRESCO cloud top heights above 14 km altitude. O22CLD cloud top heights unsurprisingly fall below those of FRESCO and ROCINN, as the O22CLD retrieval is less sensitive to cloud top heights above 10 km altitude. For optically thin volcanic ash clouds, i.e. when Earth's surface or clouds at lower altitudes shine through the volcanic ash cloud, retrieved heights fall below the volcanic ash heights derived from CALIPSO data.

Evaluation of corresponding Himawari geostationary volcanic ash height retrievals based on InfraRed (IR) brightness temperature differences (ΔBT) reveals that for this particular eruption the ΔBT volcanic ash signature - widely used for detection of volcanic ash in geostationary satellite data - changes to a ΔBT ice crystal signature for the part of the ash plume reaching the upper troposphere beyond 10 km altitude several hours after the start of the eruption and which TROPOMI clearly characterizes as volcanic ($SO_2 > 1$ DU and AAI > 4 or more conservatively $SO_2 > 10$). The presence of ice in volcanic ash clouds is known to prevent the detection of volcanic ash based on broadband geostationary satellite data. TROPOMI does not suffer from this effect, and can provide valuable and accurate information about volcanic ash clouds and ash top heights in cases where commonly used geostationary IR measurements of volcanic ash fail.

1 Introduction

Monitoring airborne volcanic ash is of crucial importance for aviation planning, as volcanic ash is an environmental hazard that can cause damage to avionics systems, abrasion of exposed airframe parts, engine damage, and even engine failure [Prata and Rose, 2015]. From early 1980s onwards there have been several well-documented damaging encounters of (jet) aircraft with volcanic ash plumes. Since then, aviation authorities have set up working groups and task forces to develop guidelines, procedures, and rules, on what to do in case of known or predicted volcanic ash [i.e. ICAO, 2012]. The advance

of satellite remote sensing techniques in the early 2000s allowed for real-time global monitoring of volcanic eruptions and airborne volcanic ash and sulfur dioxide (SO_2), like the Support to Aviation Control Service - SACS [http://sacs.aeronomie.be; Brenot et al., 2014] or the NOAA/CIMSS Volcanic Cloud Monitoring platform

35   [https://volcano.ssec.wisc.edu/]. Nevertheless, in 2010, an eruption of the Icelandic volcano Eyjafjallajökull resulted in the closure of most of the European air space, stranding more than 8.5 million people and profoundly affecting commerce [Alexander, 2013]. The total economic damage was estimated at 2.2 billion $US [Oxford Economics, 2010]. In the aftermath of the 2010 eruption of Eyjafjallajökull, aviation authorities were quick to realize that aviation guidelines for volcanic ash avoidance were too strict. Since then, guidelines have been updated [ICAO, 2012], allowing for more flexibility for aircraft

40   to maneuver around volcanic ash clouds and giving airliners more responsibility. Furthermore, it was also recommended to further develop global real-time volcanic eruption and volcanic ash monitoring services. Ongoing programs by ICAO and WMO continue to work on improving volcanic ash satellite data products that can be used for real-time monitoring of volcanic eruptions and volcanic ash clouds, as well as for tactical and strategic flight planning [ICAO, 2012; WMO SCOPE, 2015, 2018].

45   However, despite the clear need for constant monitoring of volcanic eruptions and volcanic ash clouds, and despite the availability of a wide variety of satellite remote sensing data products to meet that particular need, a centralized facility to access and analyze all available remote sensing data on volcanic eruptions and volcanic ash clouds is still lacking. This strongly hampers integration of that information into aviation operations. As a consequence, volcanic eruptions continue to pose a larger than necessary risk for aviation.

50   In order to fill this information gap, the European Union funded the EUNADICS-AV project by the European Union's Horizon 2020 research program for "Societal challenges - smart, green and integrated transport". The main objective of EUNADICS-AV is "to close the significant gap in European-wide data and information availability during airborne hazards". Volcanic clouds are one of those airborne hazards. An important aspect of EUNADICS-AV is to verify how well various satellite instrument are capable of monitoring volcanic eruptions and volcanic clouds, and how to integrate various

55   satellite data products on board a variety of satellites. This requires integrated analyses of volcanic clouds with the current suite of satellites and remote sensing data.

For more than a decade, satellite instruments like SCIAMACHY, OMI, GOME-2, OMPS, AIRS, and IASI, have been used to monitor volcanic eruptions in support of aviation. Measurements of SO_2 and the absorbing aerosol index (AAI) are currently provided in near-real-time (within 3 hours after the satellite spectral measurements) to the aviation community via

60   the SACS web-portal, which builds on the TEMIS project, which in 2003 provided the first web-based service that allowed to browse and download atmospheric satellite data products, also funded by ESA.

On 13 October 2017, ESA successfully launched the TROPOMI instrument as the single payload of ESA's S5P satellite [Veefkind et al., 2012]. TROPOMI is a grating spectrometer that measures Earth reflected radiances in the ultraviolet, visible, near infrared (NIR), and shortwave infrared (SWIR) parts of the spectrum, building on the legacy provided by the

65   satellite instruments OMI and SCIAMACHY. Already a few weeks after launch, TROPOMI started to provide promising

high spatial resolution measurements (down to 3.5×7 km2) SO$_2$, the AAI, and cloud heights from various retrieval algorithms (FRESCO, O22CLD, ROCINN).

Compared to its predecessors, TROPOMI provides measurements with a better signal-to-noise ratio and much better spatial resolution (factor 10 or more, depending on the satellite that is compared with). This allows for a much better and more

70 detailed characterization of volcanic clouds. Furthermore, due to a better spatial resolution and better instrumental signal-to-noise, TROPOMI is expected to provide improved heights of volcanic clouds, an important parameter for volcanic cloud monitoring [WMO SCOPE, 2015].

On 19 February 2018, 08:53 local time, the Indonesian volcano Mount Sinabung on Sumatra generated a dark gray plume with a high volume of ash that quickly rose to an estimated 15-17 km above sea level, according to the Darwin Volcanic Ash

75 Advisory Center (VAAC). Ash plumes were identified in satellite images, recorded by webcams and smartphones, and widely shared on social media, also because of the time of the eruption (early morning) and the clear skies at that time. The event was possibly the largest since the beginning of the current episode of unrest at Sinabung, which started in September 2013 [Smithsonian Institute, 2019].

Mount Sinabung is located in Karo Regency, North Sumatra Province (03°10′ North, 98°23.5′ East, with a height of 2460 m

80 a.s.l. [Hendrasto et al., 2012; Primulyana et al. 2017; Smithsonian Institute, Global Volcanism Program, 2019]. The stratovolcano had been dormant for more than 1200 years before it became active again in 2010, and especially since 2013 small eruptions have occurred regularly.

The 19 February 2018 Sinabung eruption provides one of the first possibilities to study the quality of TROPOMI data for volcanic cloud monitoring, also because there was a fortunate overpass of the CALIOP instrument on the Calipso satellite,

85 which is part of the A-train constellation. The TROPOMI equator crossing time of 13:30 is comparable to those of satellites in the A-train constellation.

In this paper, we evaluate satellite measurements of the 19 February 2018 Sinabung eruption with a particular focus on determining volcanic ash heights from combining TROPOMI AAI data with TROPOMI cloud height data. We also characterize the volcanic eruption plume in TROPOMI data, as well as compare TROPOMI data with geostationary

90 HIMAWARI satellite infrared data that are widely used for volcanic ash detection. TROPOMI-based volcanic ash heights are also compared with measurements from the CALIPSO satellite overpass.

2. Data

2.1 TROPOMI AAI

The AAI is a well-established data product that has been produced for several different satellite instruments spanning a

95 period of more than 30 years. The AAI was first calculated as a correction for the presence of aerosols in column ozone measurements made by the TOMS instruments [Herman et al., 1997; Torres et al., 1998], because it was observed that ozone values were too high in typical regions of aerosol emission and transport. The AAI is based on spectral contrast in the

ultraviolet (UV) spectral range for a given wavelength pair, where the difference between the observed reflectance and the modeled clear-sky reflectance results in a residual value. When this residual is positive it indicates the presence of UV-absorbing aerosols, like dust, smoke, or volcanic ash. Clouds yield near-zero residual values and negative residual values can be indicative of the presence of non-absorbing aerosols (e.g. sulphate), as shown by sensitivity studies of the AAI [e.g. de Graaf et al., 2005, Penning de Vries et al., 2009]. Unlike satellite-based aerosol optical thickness measurements, the AAI can also be calculated in the presence of clouds, so that daily global coverage is possible. This is ideal for tracking the evolution of episodic aerosol plumes from dust outbreaks, volcanic eruptions, and biomass burning. For this study, we use the TROPOMI AAI data for the wavelength pair 340-380 nm. For more details about the TROPOMI AAI retrieval algorithm, see Stein-Zweers [2016].

2.2 TROPOMI SO$_2$

Since the late 1970s, a large number of UV-visible satellite instruments have been used for monitoring anthropogenic and volcanic SO$_2$ emissions. In some cases, operational SO$_2$ retrieval streams have also been developed aiming to deliver SO$_2$ vertical column densities (VCD) in near real-time (NRT), i.e. typically with a delay of less than 3 hours.

The TROPOMI SO$_2$ retrieval algorithm is based on the DOAS technique [BIRA, 2016; Theys et al., 2017]. In brief, the log-ratio of the observed UV-visible spectrum, of radiation backscattered from the atmosphere, and an observed reference spectrum (solar or earthshine spectrum) is used to derive a slant column density (SCD), which represents the SO$_2$ concentration integrated along the mean light path through the atmosphere. This is done by fitting absorption cross-sections of SO$_2$ to the measured reflectance in a given spectral interval. In a second step, slant columns are corrected for possible biases. Finally, the slant columns are converted into vertical columns by means of air mass factors (AMF) obtained from radiative transfer calculations, accounting for the viewing geometry, clouds, surface properties, total ozone, and SO$_2$ vertical profile shapes.

2.3 TROPOMI cloud information

TROPOMI provides information about cloud properties by use of oxygen absorption in either the O$_2$A-band around 760 nm or the O$_2$-O$_2$ band around 477 nm [Veefkind et al., 2016]. In this study, we use the TROPOMI operational ROCINN cloud height [Loyola et al., 2018; Cloud as Reflecting Boundaries or CRB model] and FRESCO cloud height [Wang et al., 2008, Wang et al., 2012], both based on the O2 A-band, as well as off-line cloud height from the O22CLD algorithm based using the O$_2$-O$_2$ band. Both the FRESCO cloud height and the O$_2$-O$_2$ cloud height are based on a Lambertian cloud model. Therefore, the retrieved cloud height is the cloud mid-level rather than the cloud top [Wang et al., 2008, Sneep et al., 2012]. Note that because the current TROPOMI surface albedo databases – which rely on OMI data - are not fully representative for the TROPOMI spatial resolution and/or wavelengths, which results in inaccurate or unrealistic cloud retrievals which are flagged as missing data. It is expected that the coming years a surface albedo database will be developed based on the TROPOMI measurements itself, which should solve these retrieval artefacts.

2.4 HIMAWARI AHI

The Advanced HIMAWARI-8 Imager (AHI) is a geostationary satellite imager with 16 broad-band spectral channels from the visible to infrared portion of the electromagnetic spectrum between 0.46 μm and 13.3 μm. The sub-satellite spatial resolution of AHI is 1 km for all-but-one VIS channels and 2 km for IR channels. The HIMAWARI AHI is a multipurpose imager that provides full-disk scans of Earth every 10 minutes from a geostationary orbit at 140.7°E. The imagery can be used for a variety of applications, including general environmental monitoring (e.g. cloud-tracked winds) and numerical weather prediction [Bessho et al. 2016]. For the detection of volcanic ash, results from an ad-hoc version of the VADUGS algorithm are used [Graf et al., 2015]. The VADUGS algorithm is a neural-network based on a large number of radiative transfer simulations of geostationary infrared brightness temperatures, and retrieves the column mass load and the top altitude of volcanic ash layers. VADUGS was initially developed for SEVIRI/MSG, it has been adapted to HIMAWARI for the purpose of this paper.

2.5 CALIOP

The CALIOP lidar on board of the CALIPSO platform delivers global cloud and aerosol information. The vertical resolution of atmospheric profiles is high with 30-300m, but the horizontal sampling is poor, as the satellite is in a low-altitude earth orbit with a 16- day repeated cycle and the horizontal resolution is only 330 m to 5 km [Winker et al., 2007, 2009]. In this study, we use attenuated backscatter imagery from one CALIPSO orbit.

3. Results

3.1 Brief description of the spatiotemporal evolution of the volcanic ash cloud

The analysis of HIMAWARI AHI IR brightness temperatures and IR-based volcanic ash heights from CIMSS (Supplementary Information SI figure S1) shows that 19 February 2018 Sinabung eruption consisted of two distinct ash plumes. The initial eruption quickly reached the upper tropical troposphere (14-16 km altitude), after which the volcanic ash was transported in a north/northwesterly direction. Approximately two hours after the start of the eruption the satellite data shows lower-altitude volcanic ash (up to 6-8 km altitude) emerging from under the high altitude volcanic ash at both the northwest and southeast end of the high altitude plume. As these lower altitude plumes also move more or less in opposite direction, they more likely reflect remnants of surface pyroclastic flows and/or the eruption column collapse that are also seen in the time-lapse webcam video footage on the internet (https://youtu.be/v45J5BO_ge0).

3.2 TROPOMI

Figure 1 shows the TROPOMI FRESCO cloud height and cloud fraction, along with the TROPOMI AAI, and the AAI = 0 contour and the SO_2 = 10 Dobson Unit (DU) contour, which coincides with an approximate local time of 06:25 UTC, and 4.5

hours after the start of the eruption. By then, the volcanic plume has dispersed over an area with an approximate diameter of
160   200 km, while some parts of the volcanic ash cloud have sufficiently thinned so that cumulus clouds lower down in the
atmosphere can be identified in VIIRS imagery (see SI figure S2; note that TROPOMI flies in a so-called loose formation
with VIIRS, with a temporal separation between both of less than 5 minutes). The AAI and SO_2 contours agree well with the
extent of the volcanic plume, indicating there has not been a spatial separation between aerosols and SO_2, which is known to
sometimes happen in volcanic eruptions [Cooke et al., 2014]. Guided by the AAI and SO_2 contour lines, the ash cloud can be
165   identified in the FRESCO and ROCINN cloud heights – in particular for cloud tops above 10 km - but not in the FRESCO
cloud fraction, probably because of light absorption by ash. Comparing the cloud height with the VIIRS reflectances (SI
figure S2), the volcanic plume altitudes occur where the ash cloud is sufficiently optically thick to not show the underlying
surface and clouds.

All cloud height products show the same spatial structure with the highest clouds in the northern half of the ash plume. The
170   FRESCO and ROCINN cloud heights are rather similar. However, there are also clear differences. The FRESCO cloud
heights are systematically higher than the O22CLD cloud heights. The O22CLD data product is based on absorption of the
O_2-O_2 complex, and is less sensitive to high altitude clouds as concentrations of the O_2-O_2 complex decrease strongly above
approximately 10 km altitude [Acarreta et al., 2004]. The O22CLD algorithm is therefore computationally limited to a
maximum cloud top pressures of 150 hPa (~13) km. FRESCO and ROCINN are based on absorption of O2, whose
175   concentrations decrease much slower above 10 km altitude. The FRESCO and ROCINN cloud heights can therefore be used
up to 15 km altitude. The lower cloud height of O22CLD vs FRESCO/ROCINN is thus most likely due to the lower
sensitivity of O22CLD for high clouds.

3.3 CALIOP

Although the 19 February 2018 Sinabung eruption was small in spatial extent and rather short-lived, by mere accident there
180   was a perfect overpass with the CALIOP instrument in the A-train constellation (see Figure 1). The CALIOP track goes
straight through the core of the volcanic ash cloud and across the north-south gradient in cloud tops.

Figure 2 shows the CALIOP backscatter signal at 532 nm overlaid with the TROPOMI FRESCO cloud heights, which are
color coded according to the corresponding AAI values. The CALIOP data clearly shows a cloud/ash layer around 15 km
altitude, but also two cloud/ash structures extending from the ground up to approximately 10 km altitude, with an increase in
185   height going from south to north.

There is a good agreement between the location of enhanced TROPOMI AAI values, FRESCO cloud height, and the altitude
of high backscatter signal in the CALIOP data. The maximum cloud height in FRESCO agrees with the maximum
backscatter height in CALIOP between 4° and 5° latitude. Between 3° and 4° latitude, the FRESCO cloud height fall right in
between the CALIOP backscatter data around 15 km altitude and those close to the surface. The CALIOP data also suggests
190   that backscatter signals between 3° and 4° latitude are weaker than between 4° and 5° latitude, which might indicate less
dense ash or clouds. For a semi-transparent cloud/ash plume it could be expected that FRESCO cloud heights are lower than

the actual height of the cloud/ash plume due the presence of bright clouds nearer to the surface. Note that CALIOP's own feature mask does not identify any of these backscatter signals as aerosol: the high-altitude structures are flagged as regular clouds, and the below-cloud structure as "totally attenuated", even though clearly the attenuation is not complete.

195   Figure 3 shows the corresponding cloud heights from the O22CLD and ROCINN algorithms. The ROCINN cloud height is very similar to the FRESCO cloud height (R2 = 0.98 for FRESCO cloud heights between 0.5 and 14 km). The only difference occurs for FRESCO cloud heights > 14 km where the ROCINN cloud height appears to be nearly constant. For the O22CLD data the maximum heights are on average lower than the FRESCO/ROCINN cloud heights. The lower cloud height of the O22CLD product is likely related to the reduced sensitivity of O22CLD for clouds above approximately 10 km

200   altitude. Nevertheless, all products clearly indicate volcanic cloud heights of 10 km and higher, and all data products increasing heights in the volcanic cloud going from south to north.

Although the CALIOP overpass is perfect in space, the time difference between TROPOMI and CALIOP of approximately 45 minutes is not insignificant. It is therefore unlikely that TROPOMI and CALIOP ash layers and structures exactly match. The flow direction of the volcanic ash plume was northwards, which means that CALIOP should also be displaced north

205   compared to TROPOMI. A rough estimate of northward cloud motion based on the geostationary satellite data indicates that the displacement may be approximately 0.5°/hour, which makes it not unreasonable to assume that some of the discrepancies between TROPOMI and CALIOP could also be related to the differences in observation time. Furthermore, volcanic eruption plumes have their own dynamics, with for example pyroclastic flows near the surface which appear to travel partly in the opposite direction of the background flow. The eruption dynamics may thus have additional effects on the ash plume

210   displacement, but this cannot be investigated based on the available satellite data.

3.4 HIMAWARI

The temporal evolution of the ash plume is further investigated using Himawari geostationary IR observations. Figure 4 shows the HIMAWARI 10.8-12.0 μm channel brightness temperature differences (ΔBT) as observed between 02:30 UTC and 07:30 UTC in hourly intervals, including the TROPOMI SO_2/AAI contours shown in Figure 1. The 10.8-12.0 μm

215   channel ΔBT is the basis for geostationary IR volcanic ash retrieval algorithms [Prata, 1989], with negative ΔBT potentially indicating volcanic ash, and positive ΔBTs indicative of the presence of ice.

During the first few hours (02:30-03:30), the ash plume is clearly visible both in the ΔBTs (reddish colors) and cloud heights (whites). At 03:30 UTC, two distinct clouds have emerged with fairly negative ΔBTs: one associated also with a high cloud height, and another one further south with much lower cloud heights, likely low-altitude outflow or pyroclastic flows. From

220   04:30 UTC onwards, a third region becomes visible with high cloud heights and large positive ΔBTs (purple), more reminiscent of dense high ice clouds. This 'purple' region continues to grow and expand northward.

Figure 5 shows a comparison of TROPOMI AAI and SO_2 data with regridded HIMAWARI VADUGS ΔBTs (upper left plot). When focusing on AAI and SO_2 values, it appears that larger ΔBT values occur for smaller AAI values (< 2) and SO_2 (< 20 DU). The larger ΔBT are also associated with optically more dense clouds (see VIIRS imagery in the SI and

225 comparison of TROPOMI with CALIPSO). The lack of larger AAI and SO_2 values for larger ΔBT values therefore may reflect some kind of shielding of the volcanic ash and SO_2 by the iced upper levels of the volcanic ash cloud, or SO_2 may have been converted into sulphate.

The emergence of an IR ice/water cloud signature within the volcanic ash cloud is consistent with analysis of available video footage and pictures on social media that show signs of condensation within the ash clouds soon after the start of the

230 eruption. This is indicative of a moist troposphere in this area, which is further supported by the widespread development of (late) afternoon thunderstorms on 19 February throughout Sumatra. The eruption thus caused an increase in high altitude water vapor, either by moisture contained in the eruption itself or by the rapid vertical motions within the eruption column. The results presented here support the notion that the IR volcanic ash ΔBT signature disappears when condensed water vapor or ice forms in a volcanic ash cloud, which are known to significantly hamper IR volcanic ash retrievals [Francis et al., 2012;

235 Pavolonis et al., 2013; Zhu et al., 2017].

4. Discussion and conclusions

Analysis of measurements from the recently launched polar orbiting TROPOMI satellite - with unprecedented spatial resolution and accuracy – of the volcanic eruption of Mount Sinabung on Sumatra on 19 February 2018, has revealed that the combination of TROPOMI AAI and TROPOMI SO_2 allows for accurate identification of volcanic ash plume location. In

240 addition, under the condition that the ash plume is sufficiently thick so that clouds and the Earth surface below the ash cloud are not visible, TROPOMI cloud heights also provide accurate information about the volcanic ash cloud heights. The TROPOMI FRESCO and ROCINN cloud heights agree with CALIOP cloud top measurements for optically thick volcanic ash clouds. In passing we note that the unprecedented spatial resolution of TROPOMI allows for detection of much smaller eruptions than is currently possible with polar orbiting satellite instruments like OMPS, GOME-2, and OMI.

245 Comparison with geostationary IR volcanic ash height provides clear indications that ash height estimates using cloud heights and AAI values from UV/VIS satellites like TROPOMI may underestimate actual ash heights in case of semi-transparent volcanic ash clouds, especially in the presence of high concentrations of water vapour and for very high ash clouds. For optically thin(ner) volcanic ash clouds the TROPOMI cloud heights are a weighted mean of the ash height and heights of other clouds or the surface, and may therefore be less useful for volcanic ash height monitoring purposes. Some

250 discrepancies between TROPOMI and CALIPSO may be related due to misalignment in observation times of both satellite instruments (~ 45 minutes). In addition, indications were found of shielding of the volcanic ash plume by this ice/water near top of the volcanic ash cloud.

There are also clear indications in the geostationary IR data of the formation of water/ice near the top of the volcanic ash cloud. The analysis of geostationary satellite data for this particular case revealed that under conditions of volcanic ash

255 mixed with ice of condensed water, the geostationary IR volcanic ash ΔBT signature is lost and geostationary volcanic ash retrievals cannot identify crucial parts of the ash plume. It is worth mentioning that the temporal resolution inherent to the

geostationary orbit allows the observation of the onset and evolution of the plume, even in adverse conditions for the retrieval algorithm.

Polar orbiting satellites like TROPOMI thus may be better able to detect volcanic clouds when condensed ice/water is present in volcanic plumes, in particular when synergistically combining different satellite data products like the AAI and SO_2. Satellite measurements like those from TROPOMI measurements thus can add significant value to geostationary IR volcanic ash cloud retrievals. Furthermore, in case of sufficiently dense volcanic clouds, the cloud height data products provide accurate volcanic ash cloud heights, an important piece of information for aviation. For semi-transparent volcanic ash clouds, where the cloud top height retrievals become sensitive to other reflective surfaces below the transparent volcanic ash clouds, detection of accurate volcanic ash heights is limited.

Hence, TROPOMI cloud heights can be used for determining aerosol heights for AAI values larger than 4, and in case also SO_2 is detected such measurements should be interpreted as also containing volcanic ash (column values > 1 DU). For more conservative estimates SO_2 column values > 10 could be considered. The combination of UV/VIS cloud heights, AAI and SO_2 could also be used for other UV/VIS satellites like GOME-2, OMPS, and OMI. These results highlight the importance of the integrated use of multiple (satellite) data sources for the detection and characterization of volcanic ash, in particular for aviation purposes. This has been recognized by the European Union and is being further developed within the H2020 project EUNADICS-AV (http://www.eunadics.eu).

References

Acarreta, J. R., J. F. De Haan, and P. Stammes (2004), Cloud pressure retrieval using the O2-O2 absorption band at 477 nm, J. Geophys. Res., 109, D05204, doi:10.1029/2003JD003915.

Alexander, D. (2013). Volcanic ash in the atmosphere and risks for civil aviation: a study in European crisis management, International Journal of Disaster Risk Science, 4(1), 9-19, doi:10.1007/s13753-013-0003-0

Bessho K., and Coauthors (2016), An introduction to Himawari-8/9—Japan's new-generation geostationary meteorological satellites. J. Meteor. Soc. Japan, 94, 511−183, doi:10.2151/jmsj.2016-009

BIRA (2016), S5P/TROPOMI SO_2 ATBD, S5P-BIRA-L2-400E-ATBD, http://www.tropomi.eu/sites/default/files/files/S5P-BIRA-L2-ATBD-SO2_400E_TROPOMI_v1p0p0_20160205.pdf

Brenot, H., Theys, N., Clarisse, L., van Geffen, J., van Gent, J., Van Roozendael, M., van der A, R., Hurtmans, D., Coheur, P.-F., Clerbaux, C., Valks, P., Hedelt, P., Prata, F., Rasson, O., Sievers, K., and Zehner, C.(2014), Support to Aviation Control Service (SACS): an online service for near-real-time satellite monitoring of volcanic plumes, Nat. Hazards Earth Syst. Sci., 14, 1099-1123, doi:10.5194/nhess-14-1099-2014.

Cooke, M. C., Francis, P. N., Millington, S. , Saunders, R. and Witham, C. (2014), Detection of the Grímsvötn 2011 volcanic eruption plumes using infrared satellite measurements. Atmos. Sci. Lett., 15: 321-327, doi:10.1002/asl2.506.|

de Graaf, M., Stammes, P., Torres, O., and Koelemeijer, R.B.A. (2005), Absorbing Aerosol Index: Sensitivity analysis, application to GOME and comparison with TOMS, J. Geophys. Res. 110 (D1), doi:10.1029/2004JD005178.

290 Francis, P. N., M. C. Cooke, and R. W. Saunders (2012), Retrieval of physical properties of volcanic ash using Meteosat: A case study from the 2010 Eyjafjallajökull eruption, J. Geophys. Res., 117, D00U09, doi:10.1029/2011JD016788.

Graf, K., S. Kox, M. Schmidl, and J. Gasteiner (2015), the VADUGS algorithm, Volcanic Ash Detection using Geostationary Satellites, presentation at the WMO Intercomparison Workshop, Madison, Wisconsin, United States, 29 June – 02 July 2015.

295 http://cimss.ssec.wisc.edu/meetings/vol_ash15/PDFs/20150630/Item2.10_20150630_WMO_Madison_Graf.pdf

Hendrasto, M.,, Surono, A. Budianto, Kristianto, H. Triastuty, N. Haerani, A. Basuki, Y. Suparman, S. Primulyana, O. Prambada, A. Loeqman, N. Indrastuti, A.S. Andreas, U. Rosadi, S. Adi, M. Iguchi, T. Ohkura, S. Nakada, and M. Yoshimoto (2012). Evaluation of volcanic activity at Sinabung volcano, after more than 400 years of quiet, Journal of Disaster Research Vol, 7(1), 37, doi :10.20965/jdr.2012.p0037.

300 Herman, J. R., Bhartia, P. K., Torres, O., Hsu, C., Seftor, C., and Celarier, E. A. (1997), Global distributions of UV-absorbing aerosols from NIMBUS 7/TOMS data, J. Geophys. Res., 102, 16911–16922, doi:10.1029/96JD03680|.

ICAO (2012), Flight Safety and Volcanic Ash, ICAO Document 9974, available at: http://www.icao.int/publications/Documents/9974_en.pdf, accessed May 2018.

Loyola, D. G., Gimeno García, S., Lutz, R., Argyrouli, A., Romahn, F., Spurr, R. J. D., Pedergnana, M., Doicu, A., Molina
305 García, V., and Schüssler, O. (2018), The operational cloud retrieval algorithms from TROPOMI on board Sentinel-5 Precursor, Atmos. Meas. Tech., 11, 409-427, doi:10.5194/amt-11-409-2018.

Oxford Economics [2010], https://www.tcd.ie/Economics/assets/pdf/SER/2014/elin_thora.pdf

Pavolonis, M. J., A. K. Heidinger, and J. Sieglaff (2013), Automated retrievals of volcanic ash and dust cloud properties from upwelling infrared measurements, J. Geophys. Res. Atmos., 118, 1436–1458, doi:10.1002/jgrd.50173.

310 Penning de Vries, M. J. M., S. Beirle, S., and T. Wagner (2009) UV Aerosol Indices from SCIAMACHY: introducing the SCattering Index (SCI), Atmos. Chem. Phys., 9, 9555-9567, doi:10.5194/acp-9-9555-2009.

Prata, A. J. (1989), Infrared radiative transfer calculations for volcanic ash clouds, Geoph. Res. Lett, 16 (11), 1293-1296, 10.1029/GL016i011p01293|.

Prata and Rose, Volcanic Ash Hazards and Aviation (2015), Chapter 52 in The Encyclopedia of Volcanoes (second edition),
315 Sugurdsson et al. (eds.), ISBN: 978-0-12-385938-9.

Primulyana, S., Kern, C., Lerner, A., Saing, U. B., Kunrat, S. L., Alfianti, H., & Marlia, M. (2017). Gas and ash emissions associated with the 2010–present activity of Sinabung Volcano, Indonesia. Journal of Volcanology and Geothermal Research, 10.1016/j.jvolgeores.2017.11.018.

Smithsonian Institute, Global Volcanism Program, Sinabung volcano, accessed February 2019,
320 https://volcano.si.edu/volcano.cfm?vn=261080.

Sneep, M., J. F. de Haan, P. Stammes, P. Wang, C. Vanbauce, J. Joiner, A. P. Vasilkov, and P. F. Levelt (2008), Three-way comparison between OMI and PARASOL cloud pressure products, J. Geophys. Res., 113, D15S23, doi:10.1029/2007JD008694Stein-Zweers, D. (2016), TROPOMI ATBD of the UV aerosol index, S5P-KNMI-L2-0008-RP, http://www.tropomi.eu/sites/default/files/files/S5P-KNMI-L2-0008-RP-TROPOMI_ATBD_UVAI-v1p0p0-20160203.pdf,
325   accessed February 2019.

Theys, N., I. De Smedt, H. Yu, T. Danckaert, J. van Gent,C. Hörmann, T. Wagner, P. Hedelt, H. Bauer, F. Romahn, M. Pedergnana, D. Loyola, M. Van Roozendael (2017), Sulfur dioxide operational retrievals from TROPOMI onboard Sentinel-5 Precursor: Algorithm Theoretical Basis, Atmos. Meas. Tech., 10, 119-153, doi:10.5194/amt-10-119-2017

N. Theys, P. Hedelt, I. De Smedt, C. Lerot, H. Yu, J. Vlietinck, M. Pedergnana, S. Arellano, B. Galle, D. Fernandez, C.J.M.
330   Carlito, C. Barrington, B. Taisne, H. Delgado-Granados, D. Loyola, M. Van Roozendael (2019), Global monitoring of volcanic SO_2 degassing with unprecedented resolution from TROPOMI onboard Sentinel-5 Precursor, Nature Sci. Rep. 9, doi:10.1038/s41598-019-39279-y.

Torres, O., Bhartia, P. K., Herman, J. R., Ahmad, Z., and Gleason, J. (1998), Derivation of aerosol properties from satellite measurements of backscattered ultraviolet radiation: Theoretical basis, J. Geophys. Res., 103, 17099–17110,
335   10.1029/98JD00900|.

Veefkind, J. P., Aben, I., McMullan, K., Förster, H., de Vries, J., Otter, G., et al. (2012). TROPOMI on the ESA Sentinel-5 Precursor: A GMES mission for global observations of the atmospheric composition for climate, air quality and ozone layer applications. Remote Sensing of Environment, 120, 70–83, doi:10.1016%2Fj.rse.2011.09.027.

Veefkind, J. P., de Haan, J. F., Sneep, M., and Levelt, P. F. (2016), Improvements to the OMI O2–O2 operational cloud
340   algorithm and comparisons with ground-based radar–lidar observations, Atmos. Meas. Tech., 9, 6035-6049, doi:10.5194/amt-9-6035-2016.

Wang, P., Stammes, P., van der A, R., Pinardi, G., and van Roozendael, M.: FRESCO (2008), an improved O2 A-band cloud retrieval algorithm for tropospheric trace gas retrievals, Atmos. Chem. Phys., 8, 6565-6576, doi:10.5194/acp-8-6565-2008.

Wang, P., Tuinder, O. N. E., Tilstra, L. G., de Graaf, M., and Stammes, P.: Interpretation of FRESCO cloud retrievals in case
345   of absorbing aerosol events, Atmos. Chem. Phys., 12, 9057-9077, doi:10.5194/acp-12-9057-2012, 2012.

Winker, D. M., Hunt, W. H., & McGill, M. J. (2007). Initial performance assessment of CALIOP, Geophysical Research Letters, 34 (19), doi:10.1029/2007GL030135|.

Winker, D. M., Vaughan, M. A., Omar, A., Hu, Y., Powell, K. A., Liu, Z., W.H. Hunt, and Young, S. A. (2009). Overview of the CALIPSO mission and CALIOP data processing alhttp://www.wmo.int/pages/prog/sat/documents/SCOPE-NWC-
350   PP2_VAIntercompWSReport2015.pdfgorithms. Journal of Atmospheric and Oceanic Technology, 26 (11), 2310-2323, doi:10.1175/2009JTECHA1281.1.

WMO (2015), Final Report of the Meeting on the Intercomparison of Satellite-based Volcanic Ash Retrieval Algorithms, Madison WI, USA 29 June - 2 July 2015 .

WMO   (2017),   SCOPE   Nowcasting,   Volcanic   Ash   Algorithm   Intercomparison   -   Pilot   Project   2,
355   http://www.wmo.int/pages/prog/sat/meetings/documents/IPET-SUP-3_Doc_07-01-02_SCOPE-NWC-PP2.pdf

Zhu, L., J. Li, Y. Zhao, H. Gong, and W. Li (2017), Retrieval of volcanic ash height from satellite-based infrared measurements, J. Geophys. Res. Atmos., 122, 5364–5379, doi:10.1002/2016JD026263.

360 **Glossary**

AAI	- Absorbing Aerosol Index
AIRS	- Atmospheric InfraRed Sounder
AMF	- Air Mass Factor
AHI	- Advanced Himawari Imager
365 BIRA	- Belgian Institute for Space Aeronomy
ΔBT	- Brightness Temperature Difference
CALIOP	- Cloud-Aerosol Lidar with Orthogonal Polarization
CALIPSO	- Cloud-Aerosol Lidar and Infrared Pathfinder Satellite Observations
CIMSS	- Cooperative Institute for Meteorological Satellite Studies
370 DOAS	- Differential Optical Absorption Spectroscopy
DU	- Dobson Unit
ESA	- European Space Agency
EUNADICS-AV	- European Natural Airborne Disaster Information and Coordination System for AViation
FRESCO	- Fast Retrieval Scheme for Clouds from the Oxygen A-band
375 GOME-2	- Global Ozone Monitoring Experiment 2
ICAO	- International Civil Aviation Organization
IASI	- Infrared atmospheric sounding interferometer
IR	- InfraRed
NOAA	- National Oceanic and Atmospheric Administration
380 NRT	- Near Real Time
OMI	- Ozone Monitoring Instrument
OMPS	- Ozone Mapping Profiler Suite
O22CLD	- O_2-O_2 O_2-O_2 cloud
ROCINN	- Retrieval Of Cloud Information using Neural Networks
385 SACS	- Support for Aviation Control Service
SCD	- Slant Column Density
SCIAMACHY	- SCanning Imaging Absorption SpectroMeter for Atmospheric ChartographY
SCOPE	- Sustained, Coordinated Processing of Environmental satellite data for nowcasting
SI	- Supplementary Information
390 SO_2	- Sulfur dioxide
SUOMI-NPP	- Suomi National Polar-orbiting Partnership
S5P	- Sentinel-5 Precursor
TEMIS	- Tropospheric Emission Monitoring Internet Service

TOMS	- Total Ozone Mapping Spectrometer
395 TROPOMI	- TROPOspheric Monitoring Instrument
UTC	- Universal Time Coordinate
UV	- UltraViolet
VAAC	- Volcanic Ash Advisory Center
VADUGS	- Volcanic Ash Detection Using Geostationary Satellites.
400 VCD	- Vertical Column Density
VIS	- Visible
VIIRS	- Visible Infrared Imaging Radiometer Suite
WMO	- World Meteorological Organization

405 Figures
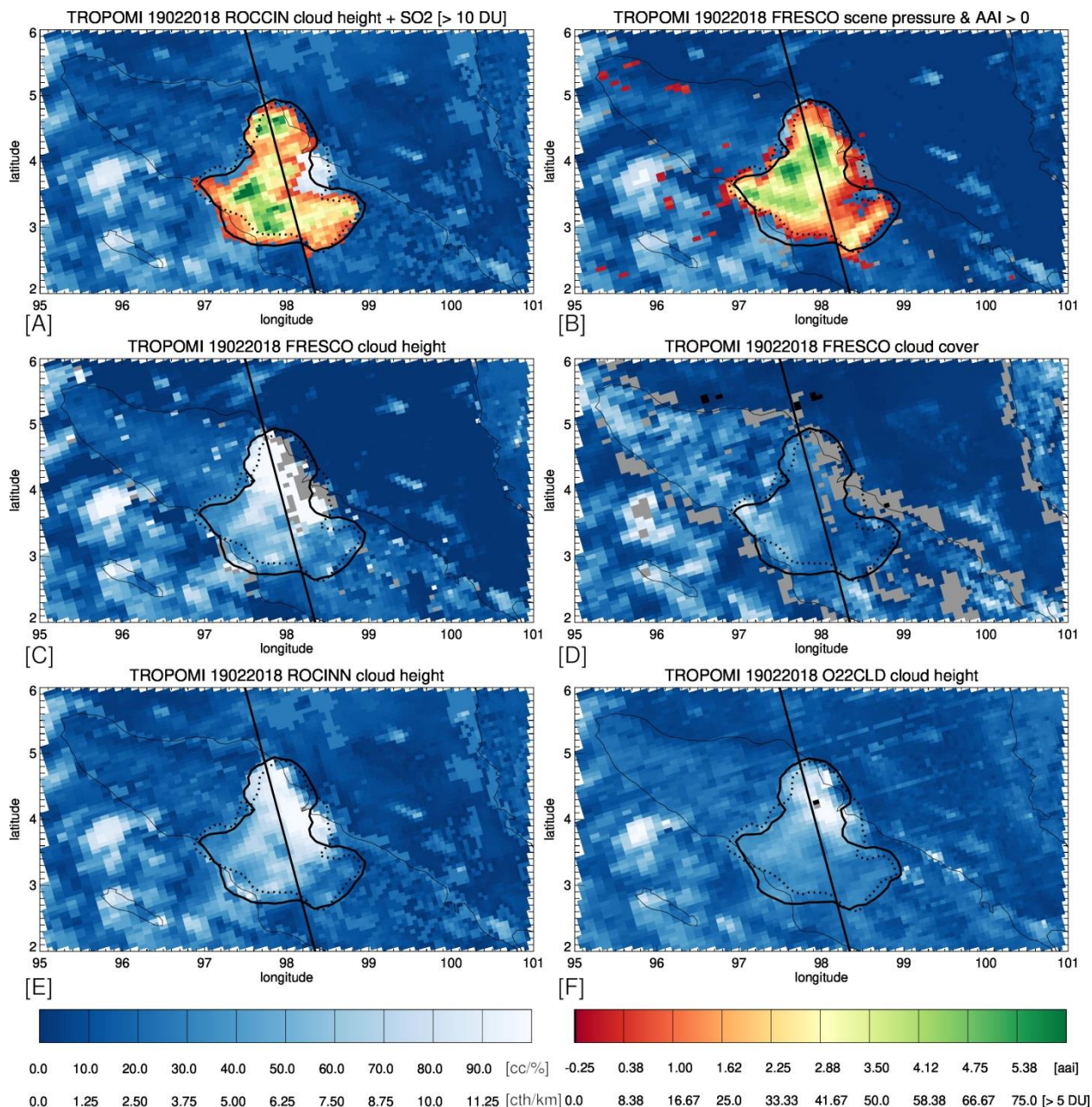
Figure 1. TROPOMI cloud heights, cloud fraction and TROPOMI SO$_2$ (panel A) and the AAI (panel B) for the overpass of

the 19 February 2018 Sinabung eruption. The straight line denotes the path of the CALIPSO overpass, the solid line shape

410 denotes the outline of > 10 DU SO_2 columns, the dotted line shape denotes the AAI > 0 value. ROCINN cloud height is

shown in panels A+E, FRESCO cloud heights in panels B+C, FRESCO cloud fraction in panel D, and O22CLD cloud

heights in panel F. Note that for FRESCO and ROCINN cloud heights certain pixels are greyed out ("no data"), related to

yet unresolved retrieval artefacts.

415
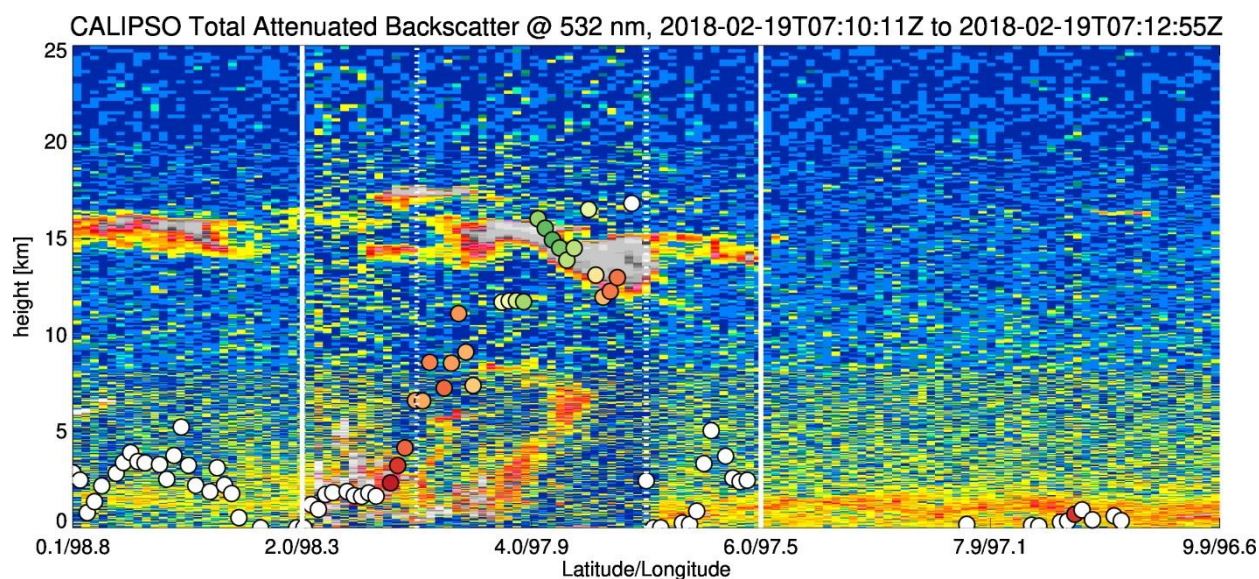
Figure 2. CALIOP total attenuated backscatter profile for the Sinabung eruption on 19 February 2018 along the track

indicated in Figure 1. The circles denote the TROPOMI FRESCO cloud heights, color coded according to the TROPOMI

AAI values as in figure 1. White dots indicate AAI values < 0.
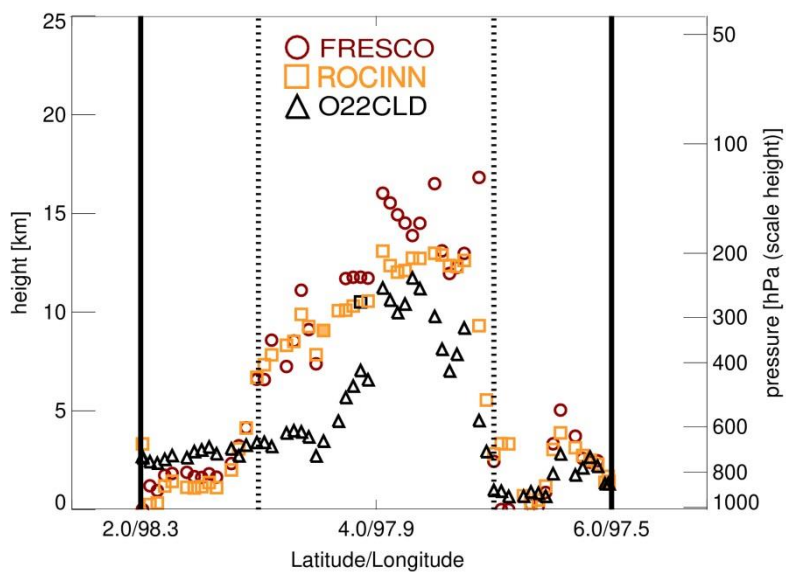
Figure 3. TROPOMI cloud heights from the FRESCO, ROCINN and O22CLD algorithms. The solid vertical lines denote the 2°N and 6°N latitudes, the dotted vertical lines the 3° and 5° latitudes. The FRESCO data is identical to the FRESCO data shown figure 2.
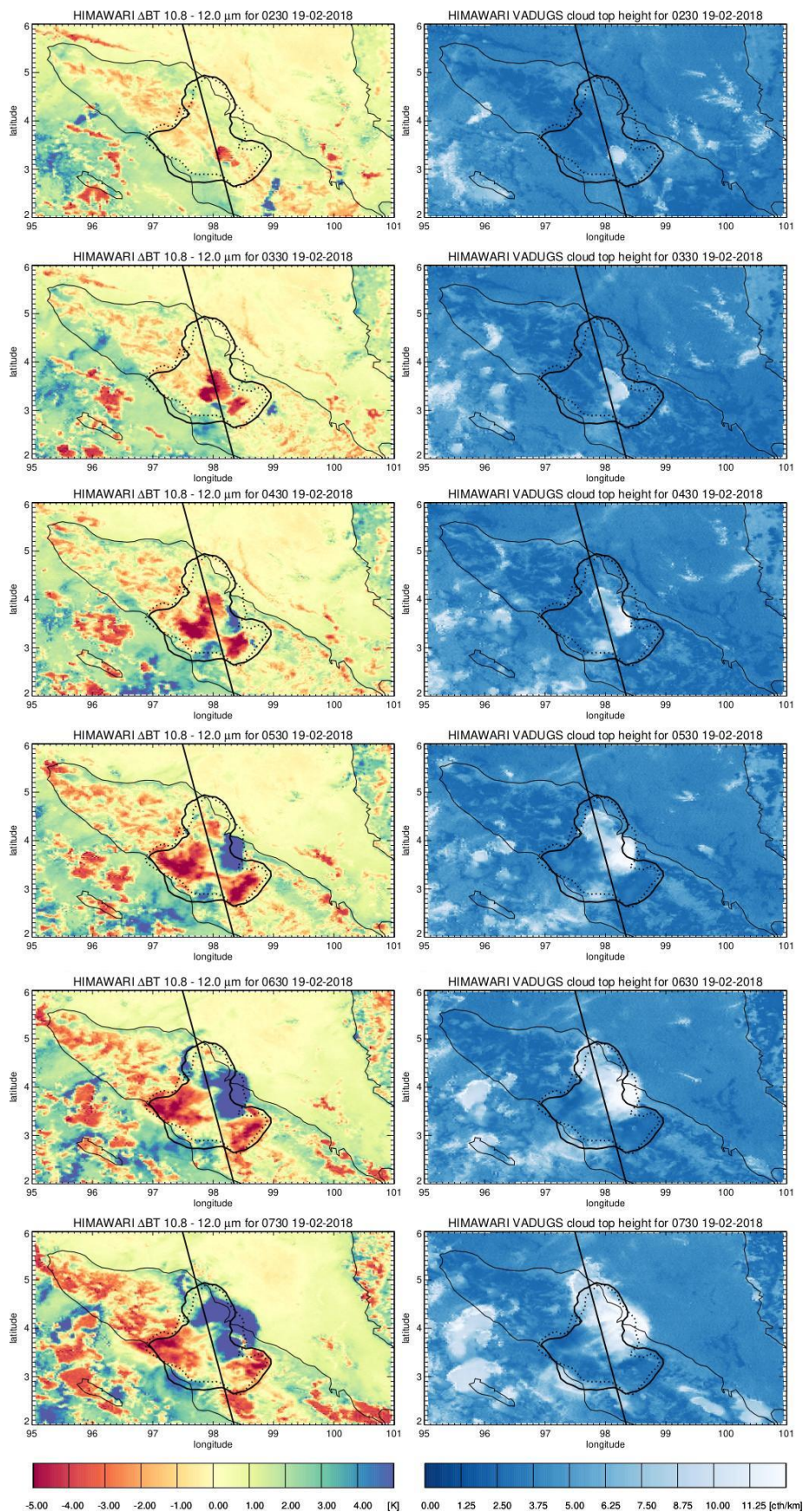
425 **Figure 4.** HIMAWARI VADUGS cloud heights (left) and 10.8-12.0 μm ΔBTs (right) for every hour between 02:30 and

07:30 UTC. The line denotes the CALIPSO overpass track. The solid and dotted contours denote outline of TROPOMI > 10

DU SO₂ columns and TROPOMI AAI > 0 value, as derived in Figure 1. Note that for the HIMAWARI ΔBTs a bias

correction of +5K is applied.
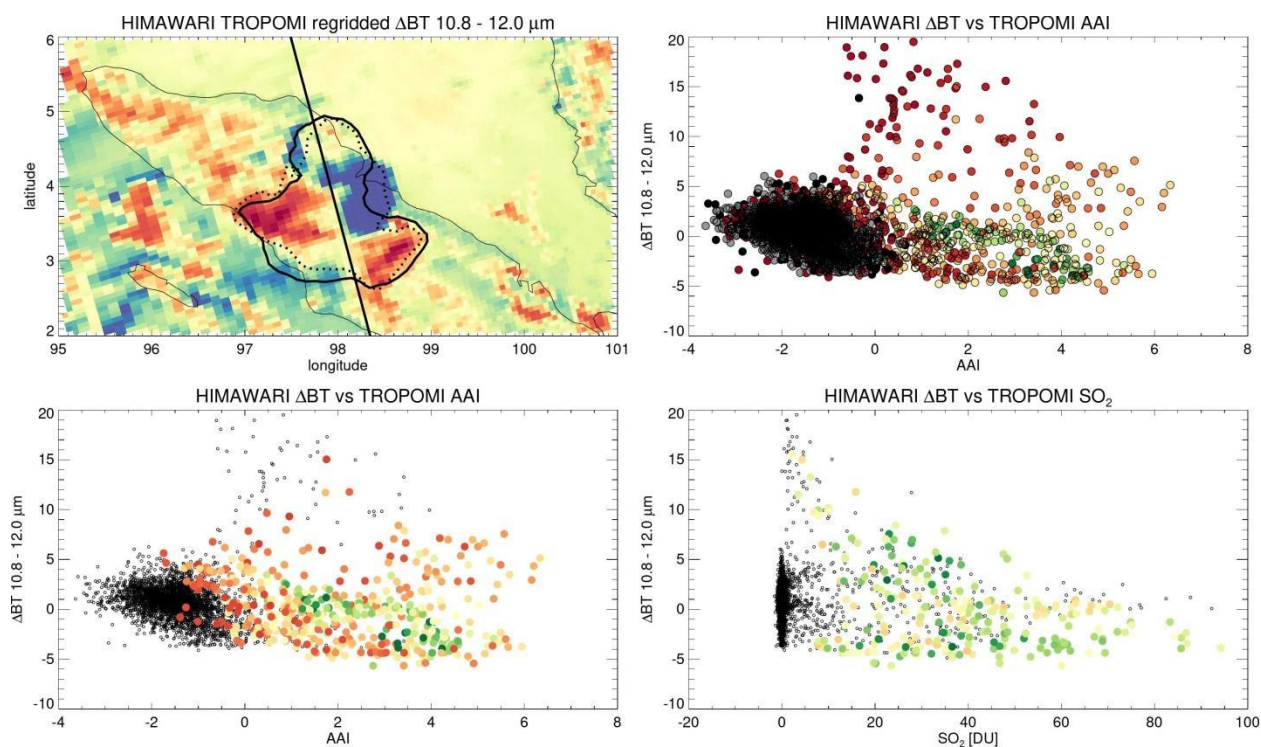
430

Figure 5. HIMAWARI ΔBTs for 19 February 2018 06:30 UTC (see Figure 4) regridded to the TROPOMI measurement grid

of that day, and correlations between the HIMAWARI ΔBTs and TROPOMI AAI and SO₂. The color coding of the dots in

the AAI scatterplots is indicative of the corresponding SO₂ value (upper right plot: SO₂ > 0 DU, lower left plot: SO₂ > 10 DU;

with green = small, red = large), and the color coding in the SO₂ scatterplot is indicative of the AAI value (AAI > 0 with

435 green = small, orange = large). The upper right plot is thus similar to the lower left plot but only pixels with SO₂ > 10 are

color coded. These color codings were added for qualitatively identifying possible relationships between ΔBT and AAI or

SO₂ within the volcanic ash plume.